Highly chemoselective hydrogenation of lactone to diol over efficient copper-based bifunctional nanocatalysts

Jun Wu[a,b], Guang Gao[a], Yong Li[b], Peng Sun[a], Jia Wang[a], Fuwei Li[a,c,*]

[a] State Key Laboratory for Oxo Synthesis and Selective Oxidation, Lanzhou Institute of Chemical Physics, Chinese Academy of Sciences, Lanzhou 730000, PR China
[b] School of Materials Science & Engineering, Shaanxi University of Science & Technology, Xi'an, 710021, PR China
[c] Dalian National Laboratory for Clean Energy, Dalian 116023, PR China

ABSTRACT

Owing to the high economic values and broad applications of diols with various alkyl chains, the development of efficient heterogeneous catalysts for the highly chemoselective synthesis of diols is highly desirable. In this work, a range of bifunctional $Cu_x/Mg_{3-x}AlO$ (x = 0.5, 1, 1.5, 2) nanocatalysts derived from layered double hydroxides (LDHs) precursors were fabricated and evaluated in the selective hydrogenation of lactones to synthesize diols. Systematic structure characterizations indicated the bifunctional catalytic sites containing active Cu nanoparticles with controllable sizes and tunable base sites could be finely constructed in the $Cu_x/Mg_{3-x}AlO$ catalysts. Intrinsic catalytic activity tests were conducted to reveal the structure-activity relationship in the model reaction of selective hydrogenation of γ-valerolactone (GVL) to produce 1,4-pentanediol (1,4-PeD); it was found that the optimal bifunctional $Cu_{1.5}/Mg_{1.5}AlO$ catalyst exhibited greatly improved catalytic activity and selectivity for this reaction, which surpassed various copper-based reference catalysts; the excellent catalytic performance of $Cu_{1.5}/Mg_{1.5}AlO$ was mainly attributed to the cooperative effect of the well-dispersed active Cu nanoparticles and the appropriate surface base sites nearby. Moreover, the bifunctional $Cu_{1.5}/Mg_{1.5}AlO$ catalyst could be extended to other lactones with different ring sizes. This work provides a low-cost, environmentally benign and atom-economic heterogeneous catalytic system for the highly selective and sustainable synthesis of value-added diols.

1. Introduction

In recent years, the diols with various alkyl chains are attracting considerable attention in both academia and industry because of their broad applications in the manufacture of polyesters, polyurethanes, fragrances and pharmaceuticals, as well as green solvents [1–3]. The selective catalytic hydrogenation of lactones is a promising and reliable route to prepare diols. Traditionally, the reduction of lactones/esters relies mostly on the use of stoichiometric amounts of metal-hydrides as reducing agents, which led to the formation of abundant waste and potential security issues [4]. The catalytic hydrogenation of lactones to diols with molecular hydrogen represented an atom-economic and environmentally benign alternative. A deal of homogeneous metal complexes catalysts have been explored for the above reactions [5–12], however, the expensive ligands and the difficult recycling problem, as well as the tedious separation (or purification) procedures, impeded their practical applications. Therefore, the development of efficient and stable heterogeneous catalysts for the highly selective hydrogenation of lactones to produce specific diols is more attractive because of its high atom- and process-economy.

Among various lactones, γ-butyrolactone (GBL) and γ-valerolactone (GVL) can be obtained from the renewable biomass resources [13]. More interestingly, GBL may also be produced *via* the hydrogenation of maleic anhydride that can be obtained by the selective oxidation of abundant butane [14,15]. Thus, they are particularly applicable for the scale production of valuable 1,4-butanediol (BDO) and 1,4-pentanediol (1,4-PeD) *via* the selective hydrogenation reactions [16–18]. However, their catalytic hydrogenation processes are challenging as a result of the difficulty in controlling the selectivity of reaction products. Advances in this field were mainly concentrated on precious metal-based catalysts as well as several copper-based catalysts [19–29]. In the case of GBL hydrogenation to produce BDO, several by-products, such as tetrahydrofuran and n-butanol, were always simultaneously generated especially using the heterogeneous catalysts with acid sites, thus leading to the low selectivity to the desired diol [19]. While for the selective hydrogenation of GVL, there are a number of possible transformation pathways, which makes the selective synthesis of 1,4-PeD even more difficult. As reported in the literature, 2-
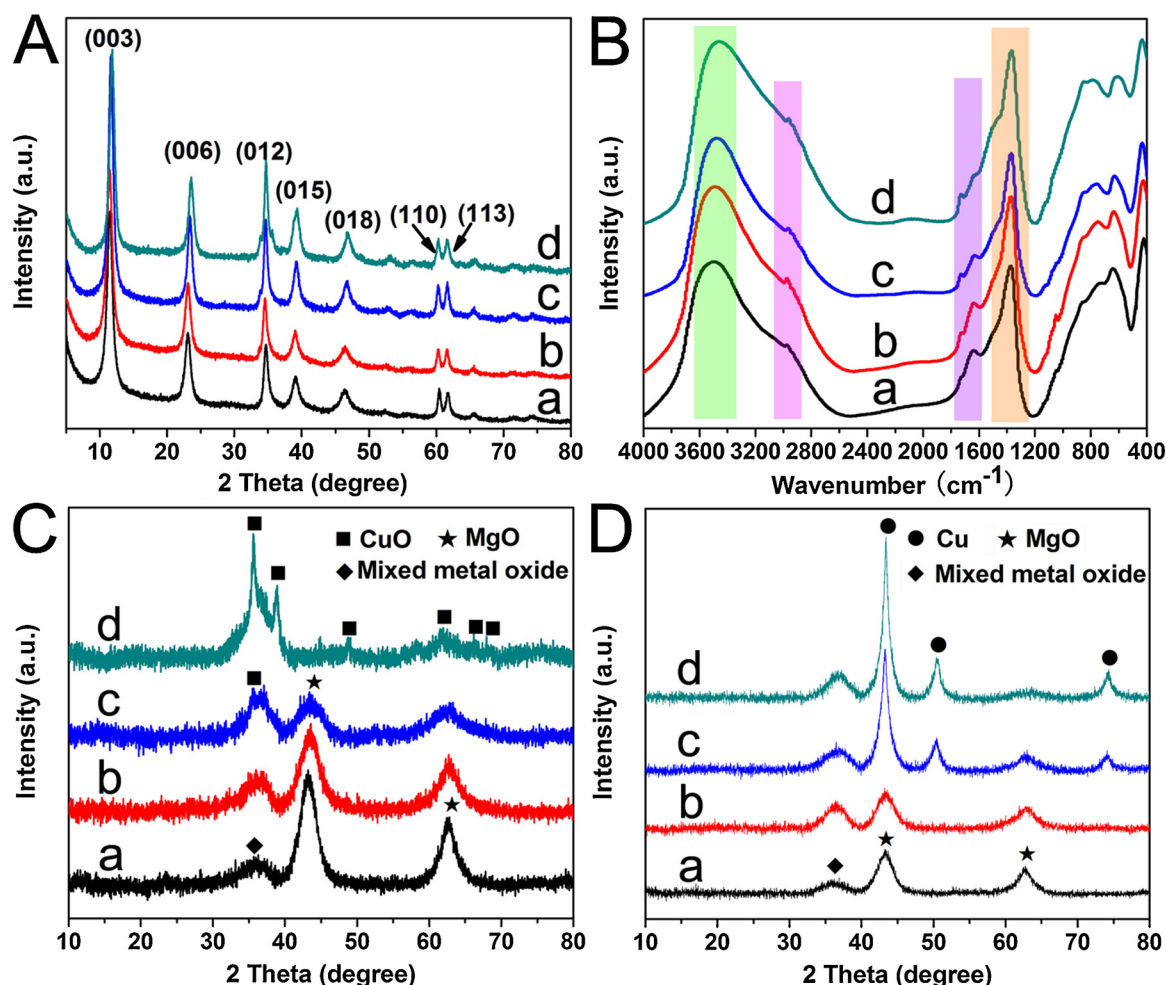

Fig. 1. (A) XRD patterns and (B) FT-IR spectra of Cu_xMg_{3-x}Al-LDH precursors; XRD patterns of (C) calcined Cu_xMg_{3-x}Al-MMO samples and (D) reduced Cu_x/Mg_{3-x}AlO catalysts with different chemical compositions (x value): (a) 0.5; (b) 1; (c) 1.5; (d) 2.

methyltetrahydrofuran (2-MTHF) was found usually accompanied with the formation of 1,4-PeD due to its easy further dehydration [24,30–33]. In the case of low-temperature calcined Cu/ZrO_2-OG catalysts, the main product of GVL hydrogenation reaction was 2-MTHF, which was attributed to the presence of large amounts of weak acid sites on these catalysts [24]. In our previous work, a small amount of 2-MTHF byproduct (selectivity: 2–7%) was also detected in the reaction of aliphatic ethyl levulinate hydrogenation to produce 1,4-PeD (catalyzed by bimetallic CuCo nanocomposite catalysts) under both batch and continuous flow conditions [34], therefore, the selectivity of 1,4-PeD still has room for improvement. In addition, the ring opening of GVL would prefer to form pentenoic acid/valeric ester over bifunctional metal/acid catalysts [16,35–37]. Our previous studies also demonstrated the acid sites could easily cause the catalyst deactivation via the deposition of coke and the alkaline additive could effectively inhibit the coke formation during the GVL hydrogenation to valeric esters [36]. Moreover, the acid-catalyst could enable the direct decarboxylation of GVL to butane [38]. Based on the above discussion, it was found that the acid sites in catalysts could easily induce the occurrence of side reactions during the hydrogenation of lactones to synthesize target diols, which would undoubtedly increase the cost of subsequent separation and purification process. Therefore, we were wondering if the replacement of frequently used metal/acid solid catalysts with metal/base bifunctional ones can improve the selectivities of the desired diols.

In this respect, two-dimensional (2D) layered double hydroxides (LDHs) seem to be suitable precursors for the fabrication of bifunctional metal/base nanocatalysts. Especially, the non-precious metal-based

bifunctional catalysts can be prepared via the two-step of calcinations and reduction process by virtue of the versatile chemical compositions of LDHs precursors [39–41]. More importantly, the homogeneous distribution of various metal species in LDHs precursors at an atomic level can help to produce well-dispersed supported metal catalysts. Besides, the particle dispersion of active metal species may be controlled by easily regulating the chemical compositions of LDHs precursors. On the other hand, the strong interaction between different metal species was favorable to improve the thermal stability of resultant catalysts [42]. Furthermore, the tunable base sites with different amounts and strengths can be controlled by introducing certain amount of alkaline component in the LDHs precursors. These unique structural characteristics make LDHs as reliable precursors of bifunctional metal/base nanocatalysts for the highly efficient and selective hydrogenation of lactones to produce diols.

Considering the superior catalytic performance of copper-based catalysts for the selective activation of various C−O bonds as well as our long-standing interest in the non-precious metal catalyzed hydrogenation reactions [34,43–53], herein, we fabricated a series of bifunctional metal/base nanocatalysts of Cu_x/Mg_{3-x}AlO with different chemical compositions derived from LDHs precursors, and their catalytic performances in the selective hydrogenation of lactones to diols were studied. The structure-activity relationship was investigated in detail by using GVL as a model lactone. It was found that, compared with varieties of copper-based reference catalysts, the optimal $Cu_{1.5}/Mg_{1.5}$AlO catalyst with well-dispersed active Cu nanoparticles and appropriate surface base sites significantly enhanced the catalytic activity and
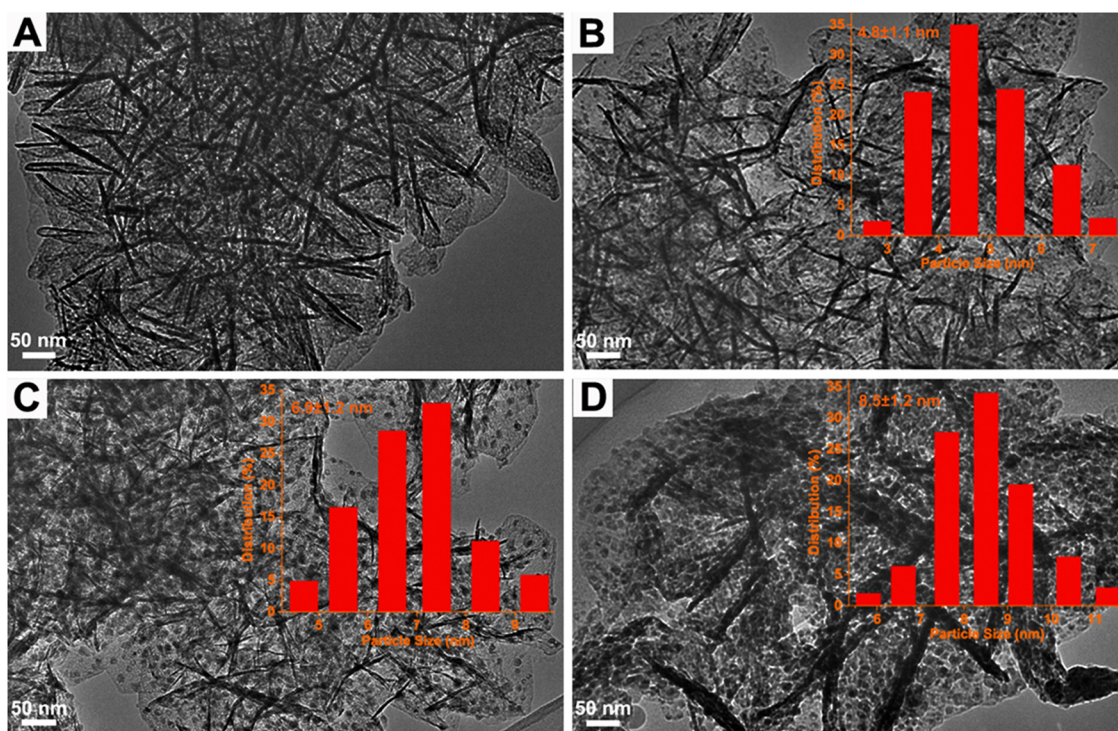
Fig. 2. TEM images of the reduced $Cu_x/Mg_{3-x}AlO$ catalysts: (A) $Cu_{0.5}/Mg_{2.5}AlO$; (B) Cu/Mg_2AlO; (C) $Cu_{1.5}/Mg_{1.5}AlO$; (D) $Cu_2/MgAlO$. The inset in (A), (B), (C) and (D) is the corresponding histogram of particle size distribution, respectively.

selectivity for the hydrogenation of GVL to produce 1,4-PeD. Moreover, our bifunctional catalysts showed good substrate tolerance that could give a number of diols with different alkyl chains.

2. Experimental details

2.1. Synthesis of catalysts

The ternary $Cu_xMg_{3-x}Al$-LDHs precursors with different Cu/Mg molar ratios $[(Cu^{2+} + Mg^{2+})/Al^{3+} = 3:1, x = 0.5, 1, 1.5, 2]$ were synthesized by using a co-precipitation method. In a typical process for the synthesis of $CuMg_2Al$-LDH, an aqueous solution containing Cu $(NO_3)_2 \cdot 3H_2O$ (30 mmol), $Mg(NO_3)_2 \cdot 6H_2O$ (60 mmol) and Al $(NO_3)_3 \cdot 9H_2O$ (30 mmol) and a NaOH (1.5 M) solution were simultaneously added into Na_2CO_3 (0.6 M) solution at room temperature under a constant pH of about 10. The resulting suspension was aged at 65 °C for 20 h. The obtained precipitate was washed with 2 L deionized water and dried at 65 °C for 24 h. Then the LDH precursor was calcined at 500 °C for 4 h in static air. The corresponding mixed metal oxide was denoted as $CuMg_2Al$-MMO. Finally, the calcined catalyst was reduced under a 20% H_2/N_2 flow at 300 °C for 3 h and the obtained catalyst was denoted as Cu/Mg_2AlO.

For comparison, a variety of Cu-based nanocatalysts (Cu: 37 wt%) loaded on various supports were fabricated by an impregnation (IM) method at 65 °C. The obtained slurry was dried at 80 °C for overnight and calcined at 500 °C for 4 h in static air. Subsequently, the resultant calcined sample was reduced at 300 °C for 3 h under a 20% H_2/N_2 flow. The reference catalysts were denoted as Cu/Mg_3AlO-IM and Cu/MO [MO = MgO, Al_2O_3, SiO_2, TiO_2, HZSM-5, Activated Carbon (AC)].

2.2. Characterization

The nitrogen adsorption and desorption isotherms (BET) of various catalysts were recorded at −196 °C on a Micromeritics ASAP 2020 equipment. Prior to each test, the sample was degassed at 200 °C overnight. Powder X-ray diffraction (XRD) profiles of the series of

catalysts were recorded with an X'Pert Promultipurpose diffractometer (PANalytical, Inc.) using Ni-filtered Cu Kα radiation (0.15046 nm) from 5° to 80° (wide angle). Cu LMM X-ray excited Auger electron spectroscopy (XAES) of the different catalysts were measured on an ESCALAB 250xi spectrometer equipped with a monochromatized Al Kα X-ray radiation source (hν = 1486.6 eV). Inductively coupled plasma atomic emission spectroscopy (ICP-AES) was used to measure the chemical compositions of the various samples on a Perkin-Elmer OPTIMA 3300 DV spectrometer (Norwalk, CT, U.S.A.). The morphology and structural properties of the catalysts were characterized with transmission electron microscopy (TEM) and energy dispersive X-ray spectroscopy (EDX) on a JEM-2010 TEM with an accelerating voltage of 200 kV. H_2 temperature-programmed reduction (H_2-TPR) profiles were measured with a unit DAX-7000 instrument (Huasi Technology Co., Ltd, China). In a typical test, the fresh precursor was firstly pretreated at 200 °C for 1 h under Ar flow. After that, the temperature was increased from room temperature to 800 °C (5 °C min^{-1}) under a 5% H_2/Ar flow (40 mL min^{-1}). The surface areas and dispersions of copper species in the different catalysts were measured by N_2O dissociative chemisorption and H_2-TPR reverse titration on a XIANQUAN TP-5080 (Tianjin, China) apparatus. Typically, the fresh catalyst precursor was firstly pretreated at 200 °C for 1 h under Ar flow (40 mL min^{-1}) and then reduced at 300 °C for 1 h in a flow of 10% H_2/N_2 (40 mL min^{-1}). After cooling down to 60 °C, the gas flow was switched to a 5% N_2O/N_2 (40 mL min^{-1}) which passed through the catalyst for 1 h to oxidize completely the surface Cu° sites to Cu_2O species. Then a second reduction process was conducted with the temperature increasing from 60 to 300 °C (5 °C min^{-1}) in 10% H_2/N_2 (40 mL min^{-1}). Finally, the surface areas and dispersions of copper speciesin the catalysts were calculated using the surface copper atomic density (1.46×10^{19} Cu atoms per m^2) and the molar stoichiometry [$2Cu(s) + N_2O \rightarrow Cu_2O(s) + N_2$ (Cu(s) refers to surface copper atom)] as well as the total number of copper atoms in the corresponding catalysts measured by ICP-AES. CO_2-TPD profiles were recorded on the XIANQUAN TP-5080 (Tianjin, China) equipment. Before each test, the fresh precursor was pretreated at 500 °C for 1 h under Ar flow and then reduced at 300 °C for 1 h under 10% H_2/N_2
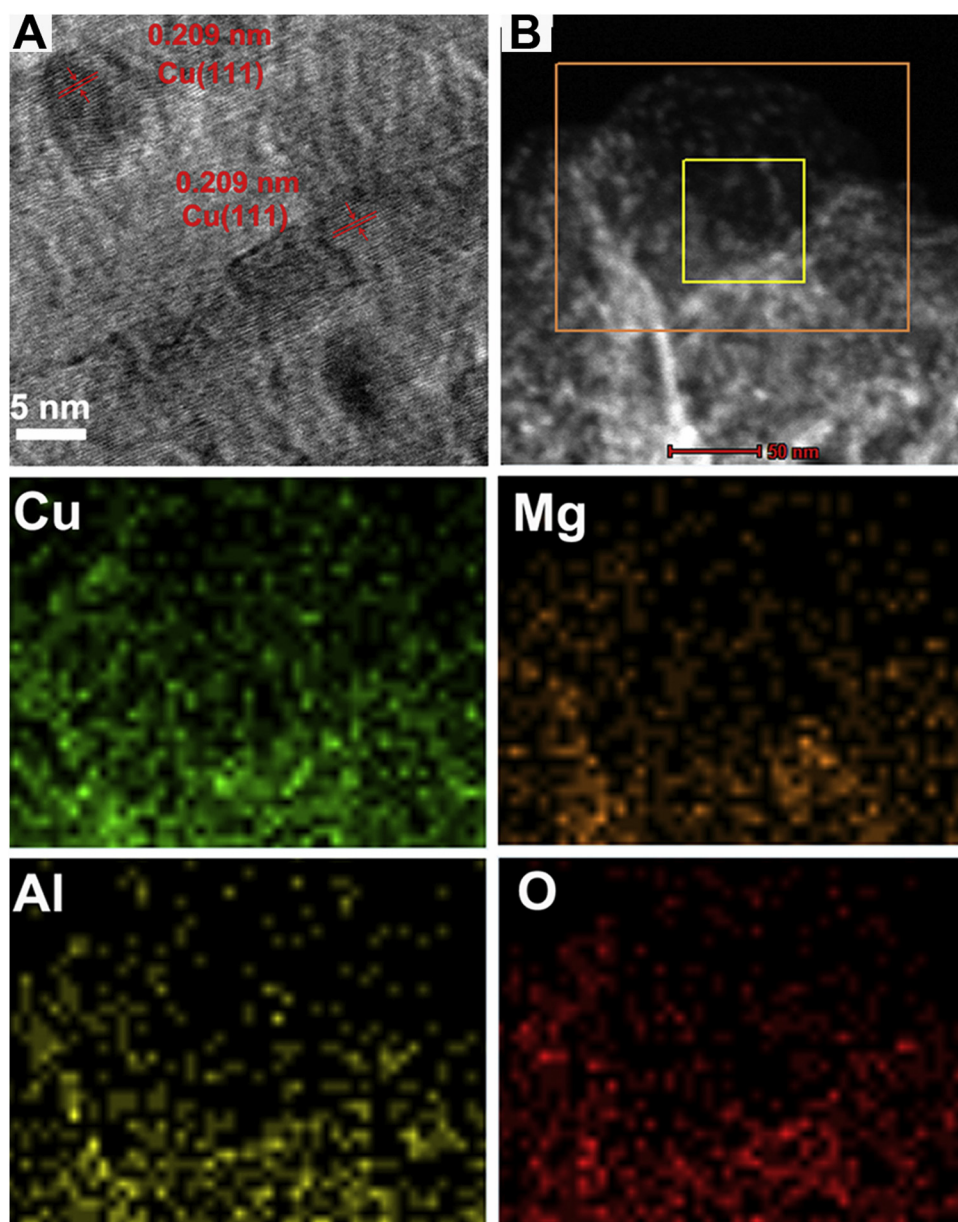
Fig. 3. Structural characterizations of the $Cu_{1.5}/Mg_{1.5}AlO$ catalyst: (A) HRTEM image; (B) HAADF-STEM image and the corresponding elemental maps of Cu, Mg, Al and O. The scale bar in (B) is 50 nm.

($40\,mL\,min^{-1}$). Afterwards, the reduced catalysts was exposed to a CO_2 flow ($40\,mL\,min^{-1}$) at 40 °C for 1 h, and then the temperature was increased to 800 °C ($10\,°C\,min^{-1}$) under a Ar flow ($40\,mL\,min^{-1}$).

2.3. Catalytic measurements

The selective hydrogenation of GVL to 1,4-PeD was selected as the probe reaction to evaluate the catalytic performance. In a typical batch reaction for the selective hydrogenation of GVL, a 100 mL stainless steel autoclave (800 rpm) was charged with 5 mmol lactone, 80 mg catalyst and 20 mL 1,4-dioxane. After the autoclave was flushed with pure H_2 for three times, the autoclave was pressured with 5 MPa H_2 and the reaction was stirred for 12 h at 160 °C. Then the reaction mixture was cooled to room temperature and the hydrogen was released. After centrifugation, the products were analyzed using a gas chromatograph mass spectrometer (GC–MS, Agilent 5975C/7890 A) equipped with a HP-5MS column. The reactant conversion and product selectivity were identified using the gas chromatograph (Agilent GC-7890 A) equipped

with a capillary column AT-SE-54 ($25\,m \times 1.5\,mm \times 0.1\,\mu m$) and FID detector.

The continuous flow reaction for the selective hydrogenation of GVL was conducted in a fixed-bed reactor. In a typical run, 2.6 g (40–60 meshes) catalyst was charged into a stainless steel tubular reactor with 8 mm inner diameter. Before reaction, the catalyst precursor was reduced in 20% H_2/N_2 flow at 300 °C for 3 h. Then the reactor was cooled to the reaction temperature of 150 °C and the hydrogen pressure was adjusted to 5 MPa. 20 wt% GVL in 1,4-dioxane and H_2 were introduced into the reactor with H_2/GVL molar ratio of 50:1. The corresponding room-temperature weight hour space velocity (WHSV) was $0.1\,h^{-1}$. The conversion of reactant and the selectivity of product were calculated using the same methods as mentioned above.
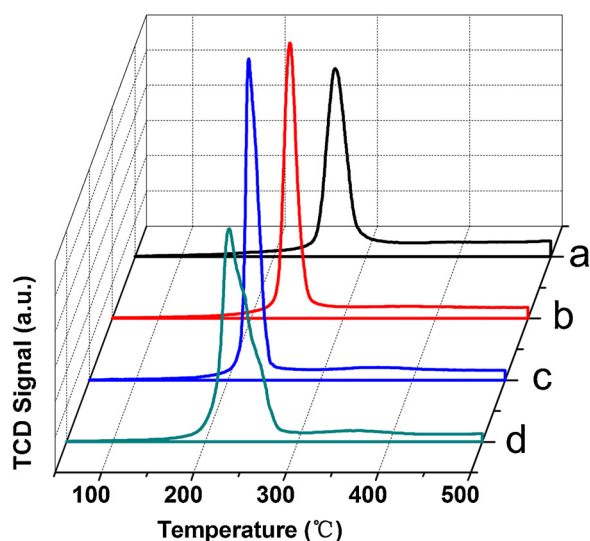
Fig. 4. H_2-TPR profiles of as-calcined $Cu_xMg_{3-x}Al$-MMO samples with different chemical compositions: (a) $Cu_{0.5}Mg_{2.5}Al$-MMO; (b) $CuMg_2Al$-MMO; (c) $Cu_{1.5}Mg_{1.5}Al$-MMO; (d) Cu_2MgAl-MMO.
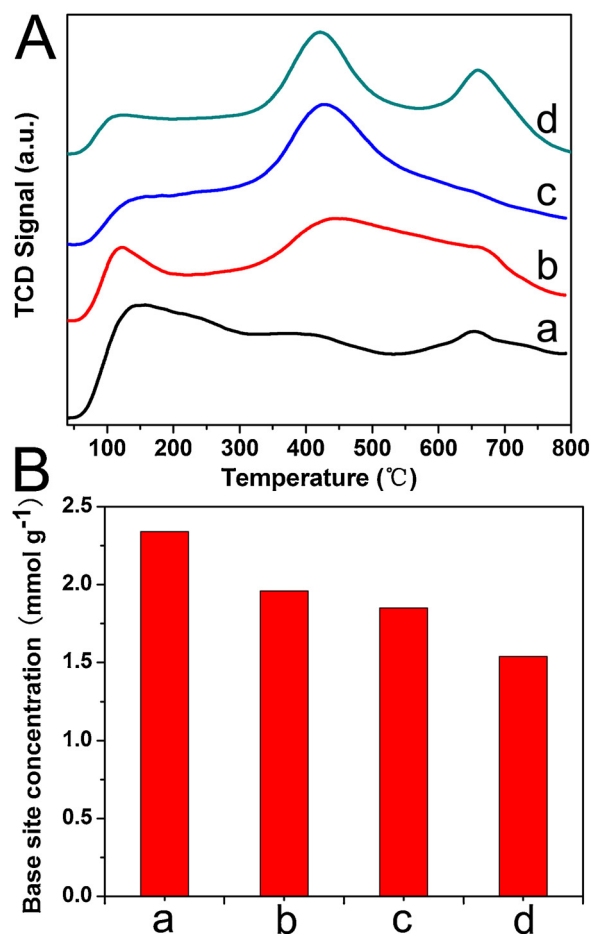

Fig. 5. (A) CO_2-TPD profiles and (B) the corresponding base site concentration of the reduced $Cu_x/Mg_{3-x}AlO$ catalysts: (a) $Cu_{0.5}/Mg_{2.5}AlO$; (b) Cu/Mg_2AlO; (c) $Cu_{1.5}/Mg_{1.5}AlO$; (d) $Cu_2/MgAlO$.

3. Results and discussion

3.1. Catalyst structural characterization

As we can see from Fig. 1A, a range of ternary $Cu_xMg_{3-x}Al$-LDHs precursors (x = 0.5, 1, 1.5, 2) with tunable chemical compositions were successfully synthesized. Evident characteristic diffraction peaks at $2\theta = 11.7°, 23.3°, 34.7°, 39.2°, 46.5°, 60.2°, 61.6°$ were attributed to (003), (006), (012), (015), (018), (110) and (113) crystal planes of two-dimensional LDH phase, respectively [54]. In addition, the structure properties of LDHs precursors with high purity were also demonstrated by FT-IR spectra. As shown in Fig. 1B, all of the LDHs precursors presented four characteristic IR bands marked by colored ribbons in the range of 4000-400 cm^{-1}. First of all, the bands around 3480 and 1640 cm^{-1} were assigned to the HOH stretching and bending vibration of physically adsorbed water, respectively [55–57]. Secondly, the small shoulder at 3050 cm^{-1} was characteristic of the hydrogen bonding of H_2O to CO_3^{2-} ions in the layer space of LDH structure [55]. Finally, a sharp band around 1376 cm^{-1} was observed, which was ascribed to the ν_3 vibration of carbonate of LDH precursor [57].

Fig. 1C presented the XRD patterns of calcined $Cu_xMg_{3-x}Al$-MMO samples. As for the oxide catalyst precursors with Cu/Mg molar ratio of 0.2, 0.5 and 1.0 (Fig. 1C, a–c), two typical diffraction peaks were observed at $2\theta = 43.0°$ and $62.7°$, which was assigned to the MgO phase [58]. Moreover, the intensities of these reflection peaks gradually diminished with the increase of Cu/Mg molar ratio. Additionally, a broad diffraction peak at about $2\theta = 36.0°$ ascribed to the mixed metal oxide phase was found in these samples [54]. Notably, no characteristic diffraction peaks of CuO species could be observed in both $Cu_{0.5}Mg_{2.5}Al$-MMO and $CuMg_2Al$-MMO precursors (Fig. 1C, a–b), indicating it was in a highly dispersed state within the mixed metal oxides. For the $Cu_{1.5}Mg_{1.5}Al$-MMO sample, a shoulder peak at $2\theta = 35.6°$ assigned to CuO phase was found. In the case of Cu_2MgAl-MMO with a high Cu/Mg molar ratio (Fig. 1C, d), several diffraction peaks belong to CuO phase were observed at $2\theta = 35.6°, 38.8°, 48.7°, 61.7°, 66.3°$ and $68.4°$ (JCPDS 45-0937). Besides, there was no diffraction peak of Al_2O_3 in all samples due to its amorphous nature. Thus, the above XRD patterns suggested that highly dispersed and tiny CuO nanoparticles could be produced *via* the topological transformation of LDHs precursors under air atmosphere.

After the reductive activation of the corresponding mixed metal oxide precursors, various $Cu_x/Mg_{3-x}AlO$ nanocatalysts were obtained. As shown in Fig. 1D, in the case of $Cu_x/Mg_{3-x}AlO$ catalysts with Cu/Mg molar ratio of 0.2 and 0.5 (Fig. 1D, a–b), a poorly-crystalline MgO phase was observed and the intensities of its reflection peaks gradually decreased. Meanwhile, the characteristic diffraction peaks of metallic Cu were not detected in the above samples as a result of the low crystallinity and high particle dispersion. With the further increase of Cu/Mg molar ratio (Fig. 1D, c–d), strong diffraction peaks ascribed to the (111), (200) and (220) crystal planes of face-centered cubic (fcc) Cu phase (JCPDS 89-2838) could be found at $2\theta = 43.4°, 50.4°$ and $74.1°$ along with the weak reflection peaks of MgO and mixed metal oxide phases in the $Cu_{1.5}/Mg_{1.5}AlO$ and $Cu_2/MgAlO$ catalysts. Moreover, the chemical states of copper species in various $Cu_x/Mg_{3-x}AlO$ catalysts were analyzed by Cu LMM X-ray excited Auger spectroscopy (Fig. S1). The deconvolution results of their corresponding Auger kinetic energy peaks indicated the presence of $Cu°$ and Cu^+ species which were located respectively around 918 and 916 eV in all of catalysts. The surface distribution of $Cu°/Cu^+$ sites ($Cu°/(Cu° + Cu^+)$ molar ratio) of $Cu_x/Mg_{3-x}AlO$ catalysts varied with their chemical compositions where the $Cu_{1.5}/Mg_{1.5}AlO$ catalyst presented the largest percentage of $Cu°$ species.

The morphology and particle distribution of Cu species in the reduced $Cu_x/Mg_{3-x}AlO$ catalysts were characterized by TEM (Fig. 2). As for the $Cu_{0.5}/Mg_{2.5}AlO$ catalyst with a low Cu loading, there was no obvious Cu nanoparticle could be identified in the TEM image, possibly owing to the small particle size and lack of contrast on the support
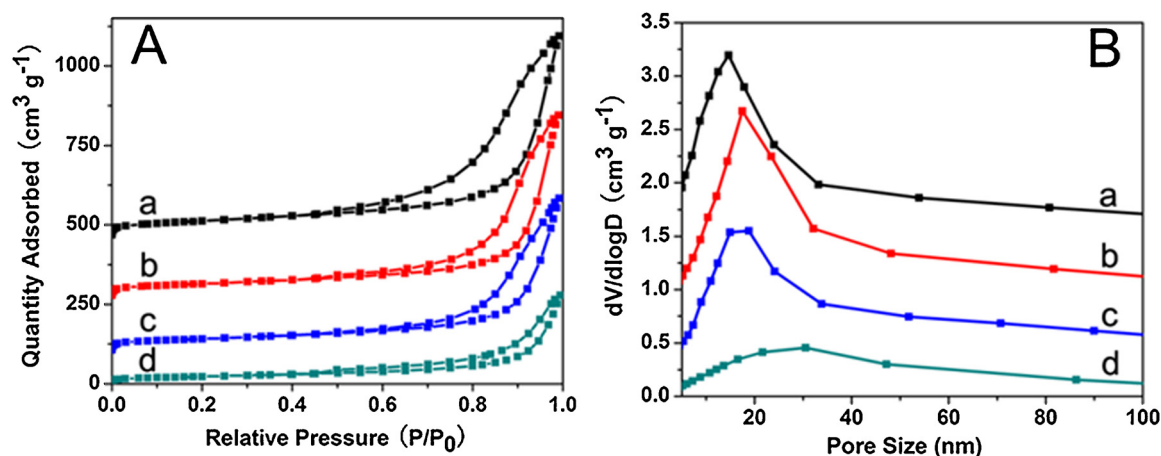
Fig. 6. (A) N_2 adsorption-desorption isotherms and (B) pore size distribution profiles of the reduced $Cu_x/Mg_{3-x}AlO$ catalysts with different Cu/Mg molar ratios: (a) $Cu_{0.5}/Mg_{2.5}AlO$; (b) Cu/Mg_2AlO; (c) $Cu_{1.5}/Mg_{1.5}AlO$; (d) $Cu_2/MgAlO$.

Table 1

Catalytic evaluation of various catalysts for the selective hydrogenation of GVL[a].

Entry	Catalyst	Conversion (%)	Selectivity (%)	
			1,4-PeD	Others[d]
1	$Cu_{0.5}/Mg_{2.5}AlO$	51	> 99	0
2	Cu/Mg_2AlO	69	> 99	0
3	$Cu_{1.5}/Mg_{1.5}AlO$	93	> 99	0
4	$Cu_2/MgAlO$	64	> 99	0
5	Cu/Mg_3AlO-IM	42	> 99	0
6	Cu/MgO	23	98	2
7	Cu/Al_2O_3	21	99	1
8	Cu/SiO_2	5	99	1
9	Cu/TiO_2	5	99	0
10	Cu/HZSM-5	6	55	45
11	Cu/AC	5	99	1
12[b]	Cu/HZSM-5	69	–	99
13[b]	$Cu_{1.5}/Mg_{1.5}AlO$	0	0	0
14	5%Pd/C	1	N.D.	N.D.
15[c]	$Cu + Mg_3AlO$	0	0	0
16	Blank	0	0	0

[a] Reaction conditions: GVL 5 mmol, catalyst 0.08 g, 1,4-dioxane 20 mL, 160 °C, H_2 5 MPa, 12 h; N.D. = Not Determined.
[b] Substrate 1,4-PeD 5 mmol.
[c] Physical mixture of Cu powder and Mg_3AlO.
[d] Others refer to the by-products including 2-MTHF, 2-butanol and other not detected.

(Fig. 2A). This phenomenon was also confirmed by the below N_2O dissociative chemisorption result (Table S1). However, with the rising of Cu loading in the catalysts, a large quantity of Cu nanoparticles with narrow size distributions were highly dispersed on the closely packed nanoflakes (Fig. 2B–D). The average particle sizes of Cu species in the different catalysts are as follows: Cu/Mg_2AlO (4.8 nm), $Cu_{1.5}/Mg_{1.5}AlO$ (6.9 nm), $Cu_2/MgAlO$ (8.5 nm). This trend was also consistent with the above XRD results (Fig. 1D). In addition, as for the supported copper-based reference catalysts fabricated with the impregnation protocol, many larger Cu nanoparticles were clearly observed on the supports (Fig. S2). This directly demonstrated the advantage of LDHs precursors which could be used to synthesize the highly dispersed supported non-precious copper-based nanocatalysts, especially, with a high metal loading.

Furthermore, the high resolution TEM (HRTEM) was used to reveal the microstructure of representative $Cu_{1.5}/Mg_{1.5}AlO$ catalyst. As shown in Fig. 3A, several nanoparticles were observed with an interlayer spacing of 0.209 nm ascribing to the (111) plane of face-centered cubic Cu lattice. On the other hand, HAADF-STEM and EDX elemental

mappings described the homogeneous distribution of Cu, Mg, Al and O in both the oxide precursor and its derived $Cu_{1.5}/Mg_{1.5}AlO$ catalyst (Fig. S3 and Fig. 3B), which suggested that the atomic-level uniform distribution of the constituent metal elements in the ternary LDHs precursors could guarantee the formation of well-dispersed copper-based nanocatalysts with high structural stability, and improve the intimacy of contact between different catalytically active sites.

In order to study the reducibility and the interaction between copper species and the support, H_2-TPR was conducted and displayed in Fig. 4. As for the $Cu_{0.5}Mg_{2.5}Al$-MMO sample (Fig. 4a), one symmetric hydrogen consumption peak centered at 267 °C was observed, ascribing to the reduction process of Cu(II) to Cu(0). With the increase of Cu/Mg molar ratio, this hydrogen consumption peak gradually shifted to a lower temperature; the corresponding reduction peaks for $CuMg_2Al$-MMO and $Cu_{1.5}Mg_{1.5}Al$-MMO samples were centered at 242 and 222 °C, respectively (Fig. 4b–c). This phenomenon suggested that the catalyst with a lower Cu/Mg molar ratio (0.2, 0.5) could enhance the strong interaction between Cu nanoparticle and mixed metal oxide supports (Fig. 4a–b) [59,60]. The $Cu_{1.5}Mg_{1.5}Al$-MMO sample with a lower reduction temperature showed the proper metal-support interaction. In addition, as for the Cu_2MgAl-MMO precursor (Fig. 4d), a shoulder peak centered at 248 °C was found, which was attributed to the reduction of bulk CuO species [59]. This result was also in accordance with the above XRD pattern (Fig. 1C, d).

The structure and distribution of surface base sites on various $Cu_x/Mg_{3-x}AlO$ catalysts were characterized by CO_2-TPD. As shown in Fig. 5A, all the catalysts presented four CO_2 desorption peaks, suggesting there were four kinds of base sites with different CO_2 adsorption strengths on the surface of catalysts. The first peak with the maximum at 130–168 °C was assigned to weak Brønsted base sites. While the second peak centered at 240–270 °C was characteristic of moderate Lewis base sites. Then the strong Lewis base sites were centered at 380–445 °C. Finally, the small desorption peak centered at 610–660 °C was attributed to super strong Lewis base sites [54,59]. In addition, the total base site concentration was calculated based on the CO_2-TPD profiles and shown in Fig. 5B. With the increase of Cu/Mg molar ratio, the surface base site concentration of the catalysts presented a gradually decreased tendency: $Cu_{0.5}/Mg_{2.5}AlO$ (2.34 mmol g^{-1}) > Cu/Mg_2AlO (1.96 mmol g^{-1}) > $Cu_{1.5}/Mg_{1.5}AlO$ (1.85 mmol g^{-1}) > $Cu_2/MgAlO$ (1.54 mmol g^{-1}). Furthermore, the distributions of base sites with different strengths varied significantly for the $Cu_x/Mg_{3-x}AlO$ catalysts. As displayed in Table S2, both the strong Lewis base sites and the total strong Lewis base sites (including the strong Lewis base sites and super strong Lewis base sites) presented a first increase and then decrease trend with the increase of Cu/Mg molar ratio, where the $Cu_{1.5}/Mg_{1.5}AlO$ catalyst had the highest amounts of strong Lewis base sites
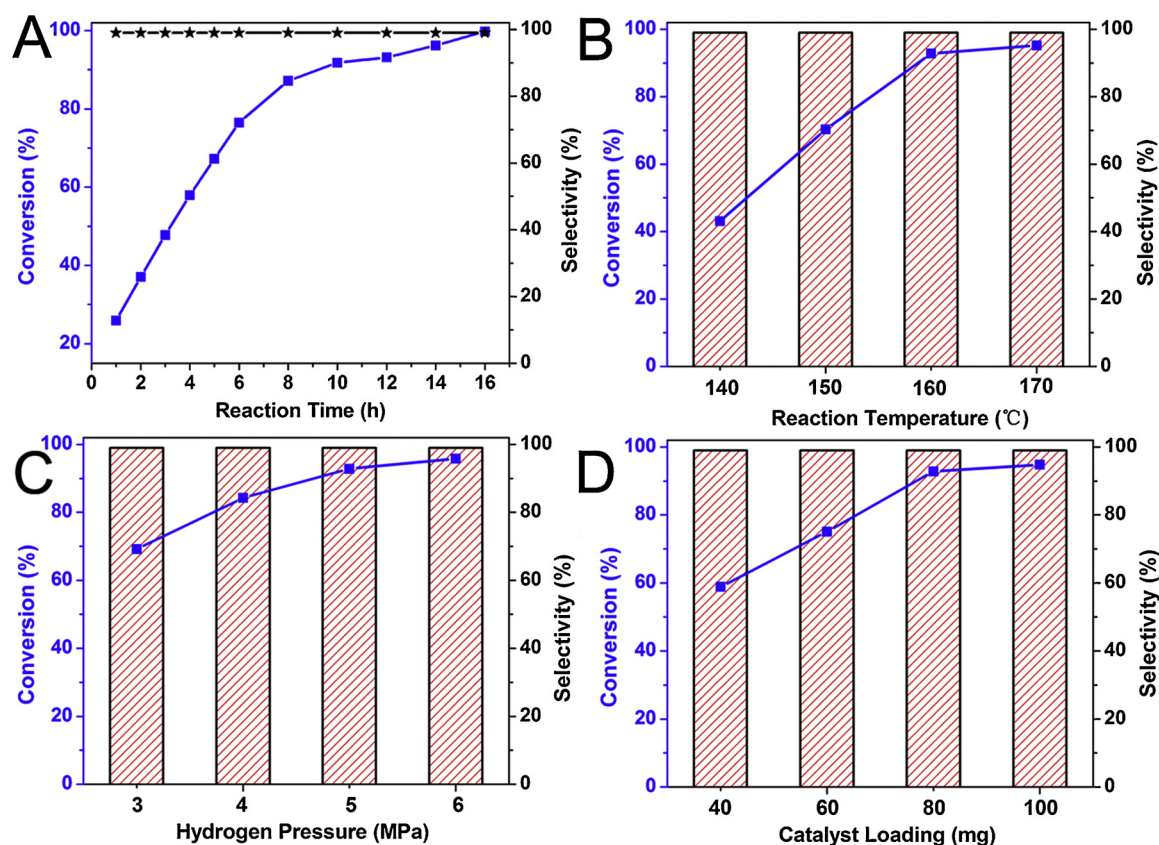
Fig. 7. (A) Kinetic study on the selective hydrogenation of GVL over $Cu_{1.5}/Mg_{1.5}AlO$ catalyst in 1,4-dioxane and the optimization of reaction parameters: (B) Effect of reaction temperature; (C) Effect of hydrogen pressure; (D) Effect of catalyst loading. Reaction conditions: (A) GVL 5 mmol, catalyst 0.08 g, 1,4-dioxane 20 mL, 160 °C, H_2 5 MPa; (B) GVL 5 mmol, catalyst 0.08 g, 1,4-dioxane 20 mL, H_2 5 MPa, 12 h; (C) GVL 5 mmol, catalyst 0.08 g, 1,4-dioxane 20 mL, 160 °C, 12 h; (D) GVL 5 mmol, 1,4-dioxane 20 mL, 160 °C, H_2 5 MPa, 12 h.

Table 2

Intrinsic catalytic performance of various $Cu_x/Mg_{3-x}AlO$ catalysts for the selective hydrogenation of GVL to 1,4-PeD[a].

Entry	Catalyst	Initial reaction rate[b] ($\mu mol\ g_{cat}^{-1}\ h^{-1}$)	TOF[c] (h^{-1})
1	$Cu_{0.5}/Mg_{2.5}AlO$	3234	3.0
2	Cu/Mg_2AlO	7632	8.0
3	$Cu_{1.5}/Mg_{1.5}AlO$	11,592	12.0
4	$Cu_2/MgAlO$	5892	6.3
5	Cu/Mg_3AlO-IM	2094	4.5

[a] Reaction conditions: GVL 5 mmol, catalyst 0.08 g, 1,4-dioxane 20 mL, 160 °C, H_2 5 MPa, 2 h.
[b] Initial reaction rate is determined from the mole of GVL converted with per gram catalyst.
[c] TOF is defined as the mole of GVL converted normalized per surface Cu site.

and total strong Lewis base sites. Therefore, the successive calcination and reduction activation of LDHs precursors were beneficial to introduce tunable amounts of base sites with different strengths, and thus effectively construct the desired bifunctional metal/base nanocatalysts.

In addition, the physicochemical properties of the $Cu_x/Mg_{3-x}AlO$ catalysts with different Cu/Mg molar ratios are shown in Table S1. ICP-AES results indicated the gradual increase of actual copper content with the rising of Cu/Mg molar ratio. The presence of mesoporous structure in $Cu_x/Mg_{3-x}AlO$ catalysts was confirmed by the series of N_2 adsorption-desorption isotherms, which showed characteristic IV isotherms with H_3-type hysteresisloops (Fig. 6A). Besides, the corresponding pore size distribution profiles revealed the pore size in these samples were mainly in the range of 10–40 nm (Fig. 6B). The BET surface areas of $Cu_x/Mg_{3-x}AlO$ catalysts diminished monotonically from 186.5 to 81.2 $m^2\,g^{-1}$

with the increase of Cu/Mg molar ratio. Moreover, the particle dispersion, metal surface area and particle size of active Cu species in the various $Cu_x/Mg_{3-x}AlO$ catalysts were examined and calculated based on N_2O dissociative chemisorption. The particle dispersions of active Cu species in the $Cu_x/Mg_{3-x}AlO$ catalysts gradually decreased from 45.1% of $Cu_{0.5}/Mg_{2.5}AlO$ to 12.0% for $Cu_2/MgAlO$. In contrast, the corresponding particle sizes exhibited a gradual increase trend, which was also consistent with the above XRD and TEM results (Fig. 1D and Fig. 2). As mentioned above, the surface textual properties and the particle dispersions of bifunctional metal/base nanocatalysts could be controlled *via* simply tuning the Cu/Mg molar ratios of the ternary LDHs precursors.

3.2. Catalytic performances

The hydrogenation of GVL to 1,4-PeD was selected as a probe reaction for studying the transformation of lactones to diols. Initially, a series of bifunctional $Cu_x/Mg_{3-x}AlO$ nanocatalysts and the supported Cu reference catalyst fabricated by the traditional impregnation method were evaluated under the identical reaction conditions. As shown in Table 1, it was found that the bifunctional $Cu_x/Mg_{3-x}AlO$ nanocatalysts exhibited highly efficient catalytic hydrogenation performance and their catalytic activities varied significantly with the Cu/Mg molar ratio (entries 1–4). In particular, the $Cu_{1.5}/Mg_{1.5}AlO$ nanocatalyst with Cu/Mg molar ratio of 1.0 showed the highest GVL conversion of 93% (entry 3), which was obviously higher than that of others. To our delight, a high selectivity of nearly 100% for the desired 1,4-PeD product was achieved over $Cu_x/Mg_{3-x}AlO$ catalysts, suggesting the rationality and effectiveness of our design for the bifunctional metal/base nanocatalysts. Furthermore, as expected, the reference supported Cu/Mg_3AlO-IM
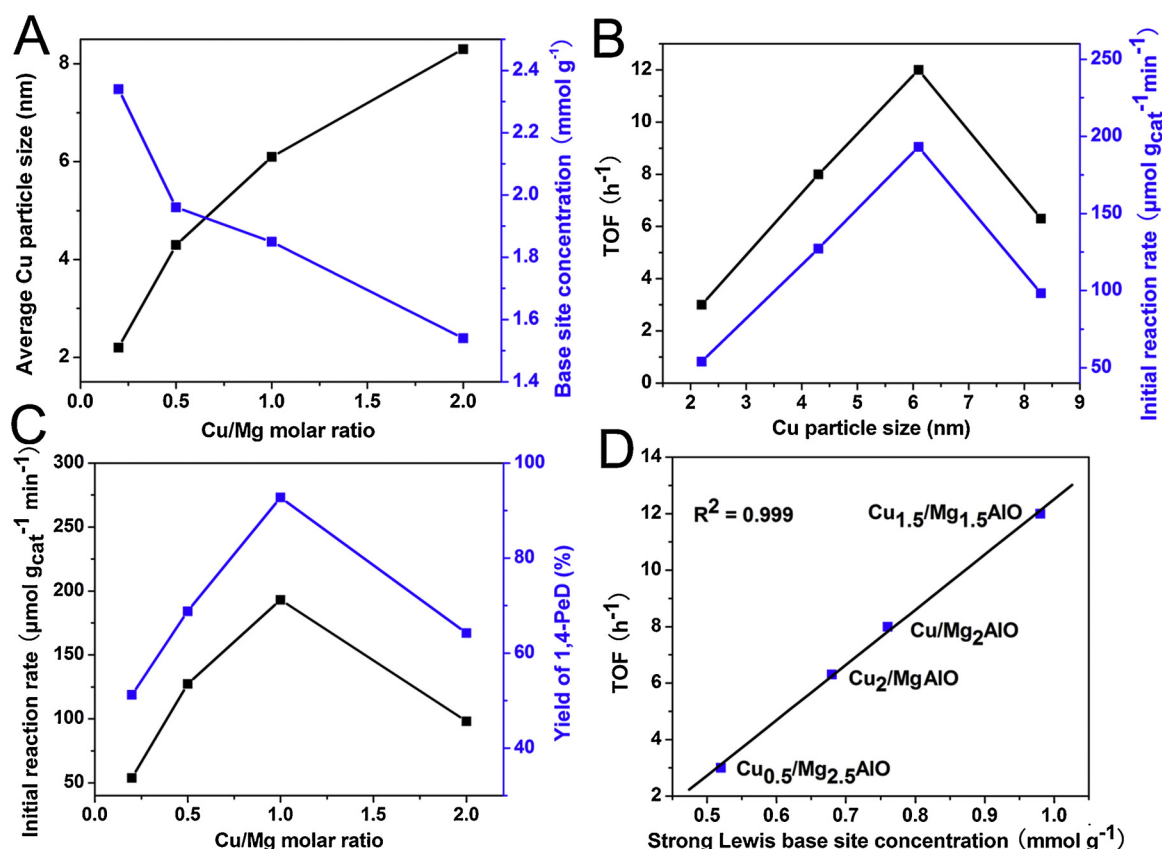
Fig. 8. (A) Relationships of average Cu particle size and base site concentration with Cu/Mg molar ratio; (B) TOF value and initial reaction rate as a function of Cu particle size; (C) Dependence of initial reaction rate and yield of 1,4-PeD on Cu/Mg molar ratio. (D) Correlation between TOF value and strong Lewis base site concentration. TOF values and initial reaction rates were calculated at the same conditions of Table 2. The yields of 1,4-PeD were calculated at the same conditions of Table 1.

Table 3
The selective hydrogenation of various lactones over $Cu_{1.5}/Mg_{1.5}AlO$ catalyst[a].

Entry	Lactone	Diol	Conversion (%)	Selectivity (%)	
				Diol	Others
1[b]			98	100	0
2[b]			92	99	0
3			99	100	0
4[b]			97	100	0
5[b]			87	99	0
6[c]			100	92	8
7[d]			93	85	15

[a] Reaction conditions: substrate 5 mmol, catalyst 0.08 g, 1,4-dioxane 20 mL, 160 °C, H_2 5 MPa, 12 h.
[b] 170 °C.
[c] 170 °C, H_2 6 MPa, 24 h.
[d] Substrate 2 mmol, 180 °C, H_2 6 MPa, 12 h.

catalyst only exhibited a 42% conversion of GVL at the same reaction conditions (entry 5), which was likely due to its obviously increased Cu nanoparticle size as evidenced by TEM (Fig. S2 A) and the non-effective contact between active Cu species and support derived from the characteristics of the impregnation protocol. This point was further confirmed by the control experiment of the physical mixture of Cu powder and Mg_3AlO as the catalyst where no conversion of GVL was observed

(entry 15).

Considering that the surface acid and base properties of the catalyst supports usually have a great influence on the catalytic activity and selectivity, several monometallic Cu reference catalysts loaded on different supports were also examined in the selective hydrogenation of GVL. Apart from the Cu/MgO and Cu/Al_2O_3 catalysts (Table 1, entries 6–7), which gave about 20% conversions of GVL, other reference supported Cu catalysts were almost inactive in the reaction (entries 8–11). Notably, in the case of Cu/HZSM-5 catalyst, large amounts (45%) of 2-MTHF and 2-butanol were detected in the product distribution (entry 10). As reported in the literature, the 2-MTHF by-product was likely derived from the further dehydration of 1,4-PeD with the assist of acid sites on the catalyst [32]. In order to demonstrate this under our catalytic system, we used 1,4-PeD as the reactant with the respective catalysis of Cu/HZSM-5 and $Cu_{1.5}/Mg_{1.5}AlO$ (entries 12–13), the result showed that a relatively high conversion of 69% for 1,4-PeD to 2-MTHF was found over the former catalyst, in contrast, no conversion of 1,4-PeD was detected over the latter catalyst, further indicating the base sites on the bifunctional nanocatalyst played a critical role in the high selectivity of desired 1,4-PeD. Moreover, the precious metal-based catalyst was examined in the hydrogenation reaction. 5% Pd/C almost showed no catalytic activity (entry 14). The result of catalyst screening indicated that our bifunctional $Cu_x/Mg_{3-x}AlO$ nanocatalysts with tunable chemical compositions were efficient candidates for the highly selective synthesis of valuable 1,4-PeD with the cooperative catalysis of well-dispersed active Cu nanoparticles and base sites nearby.

The optimal $Cu_{1.5}/Mg_{1.5}AlO$ catalyst was used for the following studies. As displayed in Fig. 7A, the kinetic investigation indicated that the conversion of GVL increased sharply to 87% in the first 8 h, then it enhanced steadily to 93% with the time extended to 12 h. Meanwhile,
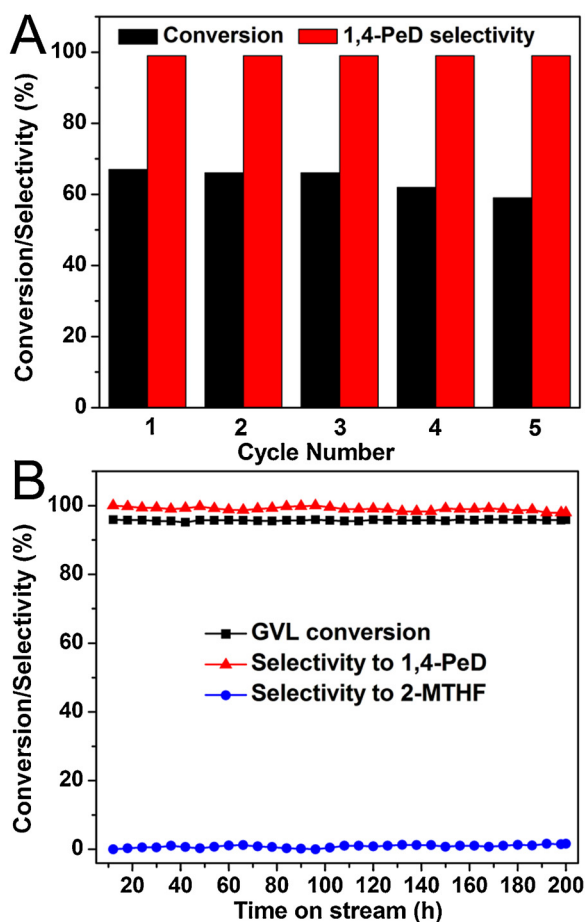
Fig. 9. Reusability of catalyst: (A) in a batch reactor and (B) in a fixed bed reactor. Reaction conditions for batch reaction: GVL 5 mmol, catalyst Cu$_{1.5}$/Mg$_{1.5}$AlO 0.08 g, 1,4-dioxane 20 mL, 160 °C, H$_2$ 5 MPa, 5 h and the conditions for continuous flow reaction: WHSV 0.1 h^{-1}, 150 °C, H$_2$ 5 MPa, H$_2$/GVL molar ratio 50.

the selectivity of 1,4-PeD was kept over 99% and no other byproducts were detected. Fig. 7B presented the GVL conversion and 1,4-PeD selectivity at the different reaction temperatures over Cu$_{1.5}$/Mg$_{1.5}$AlO catalyst, only 43% GVL conversion was obtained at the low temperature of 140 °C, and the conversion of GVL was dramatically enhanced to 93% at 160 °C, but no further increase of GVL conversion was found when reaction temperature was improved to 170 °C. Generally, the hydrogen pressure has a great effect on the hydrogenation reaction in either activity or selectivity. As shown in Fig. 7C, it can be seen that the GVL conversion elevated obviously from 69% to 93% as the hydrogen pressure increasing from 3 to 5 MPa. The GVL conversion rised linearly as the catalyst loading increased from 40 to 80 mg (Fig. 7D), suggesting the optimal amount of catalyst was 80 mg in the present reaction system.

In order to further understand the relationship between catalyst structure and catalytic activity, the intrinsic catalytic activities of the as-prepared Cu$_x$/Mg$_{3-x}$AlO and the reference catalyst were investigated. As shown in Table 2, the initial reaction rates and turnover frequency (TOF) values of various catalysts were calculated at a low GVL conversion under the reaction conditions of 160 °C, H$_2$ 5 MPa, 2 h. It should be noted that the Cu$_x$/Mg$_{3-x}$AlO nanocatalysts presented excellent intrinsic catalytic activities toward the selective hydrogenation of GVL to produce 1,4-PeD, particularly for the Cu$_x$/Mg$_{3-x}$AlO catalysts with a high Cu/Mg molar ratio (entries 2–4), their initial reaction rates and TOF values were distinctly higher than those of reference Cu/Mg$_3$AlO-IM catalyst (entry 5). Notably, the optimal Cu$_{1.5}$/Mg$_{1.5}$AlO catalyst

exhibited an approximately 6 times increase in the initial reaction rate compared with the reference catalyst (entries 3, 5). Besides, its TOF value was 2.5 times higher than that of Cu/Mg$_3$AlO-IM (entries 3, 5). It could be deduced the high catalytic efficiency of the as-prepared Cu$_x$/Mg$_{3-x}$AlO nanocatalysts probably benefited from their unique structure characteristics.

As shown in Fig. 8A, the relationships of average particle size and surface base site concentration with the Cu/Mg molar ratio of Cu$_x$/Mg$_{3-x}$AlO nanocatalysts were established. It was found that the average Cu particle size increased dramatically with the increase of Cu/Mg molar ratio while the surface base site concentration decreased gradually, which make the surface balance construction between the active Cu species and base sites easily realized by varying the chemical composition of catalysts. Furthermore, the particle size of active Cu species exerted significant influences on the intrinsic catalytic activities of Cu$_x$/Mg$_{3-x}$AlO catalysts. As illustrated in Fig. 8B, both the TOF values and initial reaction rates presented similar volcano-shape relationships with the change of average Cu particle size. The TOF value increased linearly from 3.0 h^{-1} of Cu$_{0.5}$/Mg$_{2.5}$AlO (2.2 nm) to the maximum of 12.0 h^{-1} for Cu$_{1.5}$/Mg$_{1.5}$AlO (6.1 nm) and then decreased dramatically to 6.3 h^{-1} of Cu$_2$/MgAlO (8.3 nm). On the other hand, in the case of initial reaction rate, the Cu$_{0.5}$/Mg$_{2.5}$AlO catalyst with a small average Cu particle size of 2.2 nm showed the lowest 3234 μmol g$_{cat}$$^{-1}$ h^{-1}. As the increase of particle size to 6.1 nm, the initial reaction rate enhanced remarkably to the highest 11,592 μmol g$_{cat}$$^{-1}$ h^{-1} for the optimized Cu$_{1.5}$/Mg$_{1.5}$AlO catalyst. Then, an obviously decreased initial reaction rate of 5892 μmol g$_{cat}$$^{-1}$ h^{-1} was observed on the Cu$_2$/MgAlO catalyst possessing a relatively larger Cu particle size of 8.3 nm. The remarkable size-dependent catalytic activity demonstrated the selective hydrogenation of GVL to 1,4-PeD was structure-sensitive in our catalytic system, and the Cu particle size played a significant role in determining the catalytic performance. The optimal Cu$_{1.5}$/Mg$_{1.5}$AlO catalyst with a proper active Cu particle size presented the highest catalytic performance in the lactone hydrogenation reaction. Such similar structure-activity relationship has also been found over different supported metal catalysts [61–66]. Furthermore, the change of Cu particle size could directly influence the distribution of active Cu sites with different surface chemical states. The variation of Cu°/(Cu° + Cu$^+$) molar ratio with the chemical composition of various catalysts was confirmed by the Cu LMM X-ray excited Auger spectroscopy (Fig. S1). The correlation between TOF value and Cu°/(Cu° + Cu$^+$) molar ratio was made (Fig. S4). The Cu$_{1.5}$/Mg$_{1.5}$AlO catalyst showed the largest Cu°/(Cu° + Cu$^+$) molar ratio, which played a crucial role in its high catalytic activity for the selective hydrogenation of GVL.

Besides, both the initial reaction rate and 1,4-PeD yield exhibited a similar first increase and then decrease trend with the change of Cu/Mg molar ratio (Fig. 8C), which suggested the cooperative catalysis of Cu species and base sites in the bifunctional catalysts was of great importance for the highly selective hydrogenation of GVL to 1,4-PeD. Moreover, by means of measuring the amount of strong Lewis base sites in the Cu$_x$/Mg$_{3-x}$AlO catalysts, a well linear correlation was created between the TOF value and the strong Lewis base site concentration (Fig. 8D), which directly demonstrated the strong Lewis base sites were beneficial for the excellent catalytic performance. As a result of the homogeneous distribution of constituent metal components in LDHs precursors, the bifunctional Cu$_x$/Mg$_{3-x}$AlO catalysts with highly dispersed Cu nanoparticles and tunable base sites with different strengths could be obtained. Thus, the dissociation activation of H$_2$ could be facilitated on the surface Cu° sites of highly dispersed active Cu nanoparticles. Meanwhile, the appropriate Cu$^+$ sites and the neighbouring surface base sites could possibly enhance the reactivity of ester group of GVL *via* interacting with the electron lone pair of carbonyl oxygen and the π* acceptor orbital of carbonyl carbon, respectively [67–69]. Moreover, the further dehydration reaction of 1,4-PeD and other acid sites-catalyzed side reactions could be suppressed effectively. Therefore, the well-dispersed Cu nanoparticles and the appropriate amount of

surface base sites in $Cu_{1.5}/Mg_{1.5}AlO$ nanocatalyst should account for the excellent catalytic hydrogenation performance.

Furthermore, present hydrogenation catalyst exhibited wide substrate scope. As shown in Table 3, the optimal $Cu_{1.5}/Mg_{1.5}AlO$ nanocatalyst worked efficiently for five- and six-membered lactones with or without different alkyl substitution, affording near 100% selectivity of the desired diols in excellent lactone conversions (entries 1–5). The lactone with unsaturated skeleton was also suitable for this bifunctional catalyst, providing corresponding diol with alkyl chain in a slight lower yield (92%, entry 6). Surprisingly, the hydrogenation of abnormal seven-membered lactone also proceed smoothly, 1,6-hexanediol could be obtained in 85% selectivity under modified reaction conditions (entry 7).

Finally, the optimal $Cu_{1.5}/Mg_{1.5}AlO$ was used to investigate the reusability of catalyst in the model reaction of GVL selective hydrogenation to 1,4-PeD (Fig. 9). Under the batch reaction conditions, the catalyst could be recycled for 5 times with a slight loss of activity, while no appreciable decline in the selectivity of 1,4-PeD was observed (Fig. 9A). The small decrease of catalytic activity was due to the minor aggregation of Cu nanoparticles as indicated by XRD and TEM results (Figs. S5 and S6). Under the continuous flow reaction conditions, a high selectivity above 99% to 1,4-PeD was obtained *via* GVL hydrogenation over $Cu_{1.5}/Mg_{1.5}AlO$ catalyst (Fig. 9B). Moreover, there was no obvious decrease in both catalytic activity and selectivity during the 200 h time-on-stream reaction. The excellent catalytic performance (activity and selectivity) and stability as well as the low-cost of our bifunctional nanocatalyst make it a promising candidate for the fabrication of highly value-added diols from lactones hydrogenation in industry.

4. Conclusions

In summary, we have demonstrated an effective approach for the highly selective synthesis of diol from the hydrogenation of lactone over the bifunctional $Cu_x/Mg_{3-x}AlO$ nanocatalysts derived from LDHs precursors. Systematic structural characterizations revealed the bifunctional catalytic sites including active Cu nanoparticles with controllable sizes and tunable base sites could be finely constructed in the $Cu_x/Mg_{3-x}AlO$ nanocatalysts. In the model reaction of GVL selective hydrogenation, the optimal $Cu_{1.5}/Mg_{1.5}AlO$ catalyst significantly enhanced the catalytic activity and selectivity for the synthesis of 1,4-PeD compared with various copper-based reference catalysts. Intrinsic catalytic activity measurements were conducted to study the structure-activity relationship of the catalytic system, which indicated the excellent catalytic performance of bifunctional $Cu_{1.5}/Mg_{1.5}AlO$ catalyst was mainly attributed to the cooperative effect of its well-dispersed active Cu nanoparticles and appropriate surface base sites nearby. Besides, the $Cu_{1.5}/Mg_{1.5}AlO$ catalyst showed good reusability in the selective synthesis of 1,4-PeD under both batch and continuous flow reaction conditions. Moreover, our bifunctional catalyst was efficient for the highly selective synthesis of a series of value-added diols from the lactones hydrogenation reactions. This work provided important clues for engineering environmentally benign and cost-effective non-precious metal-based bifunctional nanocatalysts for the catalytic hydrogenation reactions.

Acknowledgements

Appendix A. Supplementary data

Supplementary material related to this article can be found, in the online version, at doi:https://doi.org/10.1016/j.apcatb.2018.12.068.

References

[1] Z.B. Shen, S.J. Xie, W.Q. Fan, Q.H. Zhang, Z.K. Xie, W.M. Yang, Y.D. Wang, J.C. Lin, X.J. Wu, H.L. Wan, Y. Wang, Catal. Sci. Technol. 6 (2016) 6485–6489.
[2] J.F. Pang, M.Y. Zheng, X.S. Li, Y. Jiang, Y. Zhao, A.Q. Wang, J.H. Wang, X.D. Wang, T. Zhang, Appl. Catal. B Environ. 239 (2018) 300–308.
[3] Y. Liu, Y.L. Liu, Y. Zhang, Appl. Catal. B Environ. 242 (2019) 100–108.
[4] J. Seyden-Penne, Reductions by the Alumino- and Borohydrides in Organic Synthesis, 2nd ed., Wiley-VCH, Weinheim, Germany, 1997.
[5] T.P. Brewster, N.M. Rezayee, Z. Culakova, M.S. Sanford, K.I. Goldberg, ACS Catal. 6 (2016) 3113–3117.
[6] S. Elangovan, M. Garbe, H.J. Jiao, A. Spannenberg, K. Junge, M. Beller, Angew. Chem. Int. Ed. 55 (2016) 15364–15368.
[7] J. Yuwen, S. Chakraborty, W.W. Brennessel, W.D. Jones, ACS Catal. 7 (2017) 3735–3740.
[8] S. Werkmeister, K. Junge, B. Wendt, E. Alberico, H.J. Jiao, W. Baumann, H. Junge, F. Gallou, M. Beller, Angew. Chem. Int. Ed. 53 (2014) 8722–8726.
[9] X.H. Yang, H.T. Yue, N. Yu, Y.P. Li, J.H. Xie, Q.L. Zhou, Chem. Sci. 8 (2017) 1811–1814.
[10] N.A. Espinosa-Jalapa, A. Nerush, L.J. Shimon, G. Leitus, L. Avram, Y. Ben-David, D. Milstein, Chem. Eur. J. 23 (2017) 5934–5938.
[11] L.A. Saudan, C.M. Saudan, C. Debieux, P. Wyss, Angew. Chem. Int. Ed. 119 (2007) 7617–7620.
[12] W. Li, J.H. Xie, M.L. Yuan, Q.L. Zhou, Green Chem. 16 (2014) 4081–4085.
[13] J.C. Serrano-Ruiz, R. Luque, A. Sepúlveda-Escribano, Chem. Soc. Rev. 40 (2011) 5266–5281.
[14] T. Haas, B. Jaeger, R. Weber, S.F. Mitchell, C.F. King, Appl. Catal. A Gen. 280 (2005) 83–88.
[15] C.I. Meyer, S.A. Regenhardt, A.J. Marchi, T.F. Garetto, Appl. Catal. A Gen. 417-418 (2012) 59–65.
[16] L. Yan, Q. Yao, Y. Fu, Green Chem. 19 (2017) 5527–5547.
[17] D.L. Sun, S. Sato, W. Ueda, A. Primo, H. Garcia, A. Corma, Green Chem. 18 (2016) 2579–2597.
[18] L. Corbel-Demailly, B.K. Ly, D.P. Minh, B. Tapin, C. Especel, F. Epron, A. Cabiac, E. Guillon, M. Besson, C. Pinel, ChemSusChem 6 (2013) 2388–2395.
[19] X.R. Liu, X.C. Wang, G.Q. Xu, Q. Liu, X.D. Mu, H.C. Liu, J. Mater. Chem. A 3 (2015) 23560–23569.
[20] M.X. Li, G.Y. Li, N. Li, A.Q. Wang, W.J. Dong, X.D. Wang, Y. Cong, Chem. Commun. 50 (2014) 1414–1416.
[21] T. Fuchigami, N. Wakasa, N. Iwai, Japan Pat, JP1995/07082189A1, 1995.
[22] B. Tapin, F. Epron, C. Especel, B.K. Ly, C. Pinel, M. Besson, ACS Catal. 3 (2013) 2327–2335.
[23] D.L. Sun, T. Saito, Y. Yamada, X. Chen, S. Sato, Appl. Catal. A Gen. 542 (2017) 289–295.
[24] X.L. Du, Q.Y. Bi, Y.M. Liu, Y. Cao, H.Y. He, K.N. Fan, Green Chem. 14 (2012) 935–939.
[25] Q. Xu, X.L. Li, T. Pan, C.G. Yu, J. Deng, Q.X. Guo, Y. Fu, Green Chem. 18 (2016) 1287–1294.
[26] Z.W. Huang, K.J. Barnett, J.P. Chada, Z.J. Brentzel, Z.R. Xu, J.A. Dumesic, G.W. Huber, ACS Catal. 7 (2017) 8429–8440.
[27] K.T. Liu, J. Pritchard, L. Lu, R. van Putten, M.W.G.M.(Tiny) Verhoeven, M. Schmitkamp, X.M. Huang, L. Lefort, C.J. Kiely, E.J.M. Hensen, E.A. Pidko, Chem. Commun. 53 (2017) 9761–9764.
[28] T. Toyao, S.M.A.H. Siddiki, Y. Morita, T. Kamachi, A.S. Touchy, W. Onodera, K. Kon, S. Furukawa, H. Ariga, K. Asakura, K. Yoshizawa, K. Shimizu, Chem. Eur. J. 23 (2017) 14848–14859.
[29] J. Ullrich, B. Bernhard, ACS Catal. 8 (2017) 785–789.
[30] S.C. Patankar, G.D. Yadav, ACS Sustain. Chem. Eng. 3 (2015) 2619–2630.
[31] T. Mizugaki, K. Togo, Z. Maeno, T. Mitsudome, K. Jitsukawa, K. Kaneda, ACS Sustainable Chem. Eng. 4 (2016) 682–685.
[32] I. Obregón, I. Gandarias, A. Ocio, I. García-García, N.A. de Eulate, P.L. Arias, Appl. Catal. B Environ. 210 (2017) 328–341.
[33] Z.Q. Wang, G.Y. Li, X.Y. Liu, Y.Q. Huang, A.Q. Wang, W. Chu, X.D. Wang, N. Li, Catal. Commun. 43 (2014) 38–41.
[34] J. Wu, G. Gao, P. Sun, X.D. Long, F.W. Li, ACS Catal. 7 (2017) 7890–7901.
[35] J.P. Lange, R. Price, P.M. Ayoub, J. Louis, L. Petrus, L. Clarke, H. Gosselink, Angew. Chem. Int. Ed. 49 (2010) 4479–4483.
[36] P. Sun, G. Gao, Z.L. Zhao, C.G. Xia, F.W. Li, Appl. Catal. B Environ. 189 (2016) 19–25.
[37] W. Li, Y.Z. Li, G.L. Fan, L. Yang, F. Li, ACS Sustain. Chem. Eng. 5 (2017) 2282–2291.
[38] A.B. Kellicutt, R. Salary, O.A. Abdelrahman, J.Q. Bond, Catal. Sci. Technol. 4 (2014) 2267–2279.
[39] H. Chen, S. He, M. Xu, M. Wei, D.G. Evans, X. Duan, ACS Catal. 7 (2017) 2735–2743.
[40] S. Abelló, E. Bolshak, D. Montané, Appl. Catal. A Gen. 450 (2013) 261–274.
[41] W. Gao, C.M. Li, H. Chen, M. Wu, S. He, M. Wei, D.G. Evans, X. Duan, Green Chem. 16 (2014) 1560–1568.
[42] S. Kai, M.M. Lu, S.P. Xu, C.Q. Chen, Y.Y. Zhan, D.L. Li, C. Au, L.L. Jiang,

K. Tomishige, Appl. Catal. B Environ. 239 (2018) 324–333.

[43] J. Wu, G. Gao, J.L. Li, P. Sun, X.D. Long, F.W. Li, Appl. Catal. B Environ. 203 (2017) 227–236.

[44] B. Zhang, Y. Chen, J.W. Li, E. Pippel, H.M. Yang, Z. Gao, Y. Qin, ACS Catal. 5 (2015) 5567–5573.

[45] M. Behrens, F. Studt, I. Kasatkin, S. Kühl, M. Hävecker, F. Abild-Pedersen, S. Zander, F. Girgsdies, P. Kurr, B.L. Kniep, M. Tovar, R.W. Fischer, J.K. Nørskov, R. Schlögl, Science 336 (2012) 893–897.

[46] M. Tamura, T. Kitanaka, Y. Nakagawa, K. Tomishige, ACS Catal. 6 (2016) 376–380.

[47] Y.F. Zhu, X. Kong, X.Q. Li, G.Q. Ding, Y.L. Zhu, Y.W. Li, ACS Catal. 4 (2014) 3612–3620.

[48] J.L. Gong, H.R. Yue, Y.J. Zhao, S. Zhao, L. Zhao, J. Lv, S.P. Wang, X.B. Ma, J. Am. Chem. Soc. 134 (2012) 13922–13925.

[49] J. Ding, T. Popa, J.K. Tang, K.A. Gasem, M.H. Fan, Q. Zhong, Appl. Catal. B Environ. 209 (2017) 530–542.

[50] J. Yuan, S.S. Li, L. Yu, Y.M. Liu, Y. Cao, H.Y. He, K.N. Fan, Energy Environ. Sci. 6 (2013) 3308–3313.

[51] Z. Gao, C.Y. Li, G.L. Fan, L. Yang, F. Li, Appl. Catal. B Environ. 226 (2018) 523–533.

[52] Q. Hu, L. Yang, G.L. Fan, F. Li, J. Catal. 340 (2016) 184–195.

[53] W. Li, G.L. Fan, L. Yang, F. Li, Green Chem. 19 (2017) 4353–4363.

[54] S.Y. Zhang, G.L. Fan, F. Li, Green Chem. 15 (2013) 2389–2393.

[55] J. Pérez-Ramírez, G. Mul, J.A. Moulijn, Vib. Spectrosc. 27 (2001) 75–88.

[56] X. Kong, R.X. Zheng, Y.F. Zhu, G.Q. Ding, Y.L. Zhu, Y.W. Li, Green Chem. 17 (2015) 2504–2514.

[57] I. Melián-Cabrera, M.L. Granados, J.L.G. Fierro, Phys. Chem. Chem. Phys. 4 (2002) 3122–3127.

[58] J. Liu, W.H. Bing, X.G. Xue, F. Wang, B. Wang, S. He, Y.K. Zhang, M. Wei, Catal. Sci. Technol. 6 (2016) 3976–3983.

[59] H.W. Liu, Q. Hu, G.L. Fan, L. Yang, F. Li, Catal. Sci. Technol. 5 (2015) 3960–3969.

[60] C.M. Li, J.Y. Zhou, W. Gao, J.W. Zhao, J. Liu, Y.F. Zhao, M. Wei, D.G. Evans, X. Duan, J. Mater. Chem. A 1 (2013) 5370–5376.

[61] S. Wang, K.H. Yin, Y.C. Zhang, H.C. Liu, ACS Catal. 3 (2013) 2112–2121.

[62] L.C. Bai, X. Wang, Q. Chen, Y.F. Ye, H.Q. Zheng, J.H. Guo, Y.D. Yin, C.B. Gao, Angew. Chem. Int. Ed. 55 (2016) 15656–15661.

[63] J.N. Kuhn, W. Huang, C.K. Tsung, Y. Zhang, G.A. Somorjai, J. Am. Chem. Soc. 130 (2008) 14026–14027.

[64] V.V. Pushkarev, N. Musselwhite, K. An, S. Alayoglu, G.A. Somorjai, Nano Lett. 12 (2012) 5196–5201.

[65] M. Cargnello, V.V. Doan-Nguyen, T.R. Gordon, R.E. Diaz, E.A. Stach, R.J. Gorte, P. Fornasiero, C.B. Murray, Science 341 (2013) 771–773.

[66] S.W. Cao, F.F. Tao, Y. Tang, Y.T. Li, J.G. Yu, Chem. Soc. Rev. 45 (2016) 4747–4765.

[67] A.Y. Yin, X.Y. Guo, W.L. Dai, K.N. Fan, J. Phys. Chem. C 113 (2009) 11003–11013.

[68] H.L. Liu, Z.W. Huang, Z.B. Han, K.L. Ding, H.C. Liu, C.G. Xia, J. Chen, Green Chem. 17 (2015) 4281–4290.

[69] S.E. Denmark, G.L. Beutner, Angew. Chem. Int. Ed. 47 (2008) 1560–1638.